Quantifying the Pathways Modulated by Deep Brain Stimulation for Essential Tremor Using Computational Modeling

A THESIS
SUBMITTED TO THE FACULTY OF THE GRADUATE SCHOOL
OF THE UNIVERSITY OF MINNESOTA
BY

Maureen Keane

IN PARTIAL FULFILLMENT OF THE REQUIREMENTS
FOR THE DEGREE OF
MASTER OF SCIENCE

Dr. Matthew Johnson

December 2011

December 2011

Acknowledgements

I would like to thank my adviser, Dr. Matthew Johnson of the Biomedical Engineering Department. His guidance and support have been imperative in this research as well as in my development as an engineer. Additionally, I would like to acknowledge the work of Steve Deyo, an undergraduate in the Biomedical Engineering Department. Steve was integrally involved in this research study and participated in all stages of the work. He contributed significantly to this work, and I appreciate his contribution. I also acknowledge the support of Dr. Jawad Bajwa of United Hospital who contributed feedback, guidance, and data to this study. Also, I thank the Minnesota Super Computing Institute for providing the computational resources needed in this study.

Furthermore, I would like to thank Dr. Netoff and Dr. Lim of the Biomedical Engineering Department for both supporting my education as well as my research and also for serving as members of my committee. Finally, I would like to thank fellow lab members Allison Connolly, Kevin Mohsenian, and Karlo Malaga for their support and technical assistance.

Abstract

Deep brain stimulation (DBS) within or near the ventral intermediate nucleus of thalamus (Vim) is known to exert a therapeutic effect on postural and kinetic tremor in patients with Essential Tremor (ET). For patients with DBS leads placed near the caudal border of Vim, however, there is an increased likelihood of inducing paresthesias through activation of the sensory ventral caudal (Vc) nucleus of thalamus. The aim of this computational modeling study was to provide a patient-specific modeling framework for comparing the current steering abilities of the clinical Medtronic 3389 DBS lead to a novel DBS lead with directionally-oriented electrodes (dDBS). We developed patient-specific computational neuron models from three ET patients implanted with a Medtronic 3389 DBS lead. Multi-compartment models of Vim / Vc thalamocortical neurons and cerebellothalamic / medial lemniscal axonal afferents were simulated in the context of patient-specific anatomies, lead placements, and programming parameters. Complete suppression of tremor was associated with stimulating the axonal output from an average of 62.4% of Vim afferents (n=10), and persistent paresthesias were associated with activation of 35.3% of Vc afferents (n=12). The dDBS models demonstrated superior targeting of cerebello-thalamo-cortical pathways, enabling one to selectively modulate Vim and avoid activation of Vc. For patients with leads positioned near the Vc nucleus of thalamus, dDBS may allow clinicians to more selectively modulate pathways within and near the thalamus in order to achieve better therapy without inducing side effects.

Table of Contents

List of Tables

List of Figures

Introduction

Essential tremor (ET) is the most common adult movement disorder, affecting an estimated 4% of adults over the age of 40 (Louis et al. 1998). Motor symptoms of ET emerge as postural and kinetic tremors (4-12 Hz) primarily in the upper extremities and head (Whaley et al. 2007). While pharmacological therapies are known to reduce such tremors, approximately one-third of ET patients are refractory to medication (Zesiewicz et al. 2010). For these patients, deep brain stimulation (DBS) can be a fully effective surgical therapy. However, positive outcomes of this neurosurgical procedure are highly dependent on proper placement of the DBS lead in or near the cerebellar-receiving area of thalamus (ventral intermediate nucleus, Vim) (Lozano 2000).

The ideal DBS lead placement for alleviating symptoms of ET is a matter of debate as the neural mechanisms underlying these symptoms are not well understood (Jenkins et al. 1993). Pathological spike activity within the Vim is characterized by neuron 'burstiness,' demonstrating coherence with tremor frequency (Hua et al. 1998), but the central oscillator involved in this pathogenesis has not been identified. One hypothesis is that tremor activity may originate in the Guillain Mollaret triangle of the brainstem, which includes the red nucleus, the dentate nucleus, and the inferior olivary nucleus (Zesiewicz et al. 2010). Evidence demonstrates synchronized 4-12Hz oscillations in the inferior olivary nucleus, which supports the hypothesis that the olivary nucleus is the origin of the tremor activity (Plaha et al. 2006). Increased electrotonic coupling between dendrites of inferior olivary neurons may cause the abnormal oscillations. Moreover, the Purkinje cells of the cerebellum are thought to play an important role in transmitting the abnormal oscillatory activity to the dentate nucleus followed by the thalamus (Plaha et al. 2006). Reports of axonal swelling of Purkinje cells in Essential Tremor patients supports the idea that the cerebellum is involved in the central oscillatory activity of tremor (Zesiewicz et al. 2010).

Furthermore, imaging studies have been performed on patients with ET in an attempt to relate increased glucose metabolism or regional blood flow to origins of tremor activity during movements. One such study attributed the abnormal oscillatory activity to the olivary nucleus as glucose hypermetabolism was only apparent in the medulla (location of olivary nucleus) and thalamus but not in the cerebellum (Hallett and

Dubinsky 1993). On the other hand, the study performed by Jenkins et al, which used PET imaging, attributed the origin of tremor activity to the cerebellum as they reported increased cerebellar activity at rest and during movement in patients with ET (Jenkins et al. 1993). Future work to identify the central oscillator involved in tremor activity may lead to an improvement in symptom treatment.

Previous studies have noted that improvement in tremor symptoms can be obtained by either stimulating through electrodes within Vim (Benabid et al. 1991; Kobayashi et al. 2010) or slightly ventral to Vim (Barbe et al. 2011a; Herzog et al. 2007; Sandvik et al. 2011). These clinical observations suggest that there may be multiple therapeutic targets for managing Essential tremor, including the thalamo-cortical tract extending from Vim to cortex and the cerebellothalamic tract entering Vim. In the first case, DBS is thought to override neuronal tremor-burst activity in Vim (Hua et al. 1998) by generating a regular, high frequency output from Vim (Birdno et al. 2008). In the second case, DBS is thought to drive high frequency stimulation input into Vim, thereby disfacilitating tremor-burst activity in Vim (Birdno et al. 2011). With improved imaging techniques, it is possible to develop patient-specific neuron models of DBS to investigate how modulation of specific pathways relates to clinical improvement in tremor symptoms and to the induction of untoward side-effects (Butson et al. 2007).

After verifying the intended DBS target trajectory through MR or CT imaging techniques, correct placement of a DBS lead in patients with Essential tremor can typically be identified by suppression of tremor in the upper limb and face but also by transient paresthesias induced in the fingers and/or face (Benabid et al. 2004). The typical DBS lead trajectory is made along the border of Vim and the pallidal-receiving area of thalamus (nucleus ventral oral posterior, Vop) to prevent current from spreading posterior to the sensory nucleus of thalamus (ventral caudal, Vc). Extremely posterior placements of the stimulating electrode can modulate a significant portion of Vc, inducing persistent paresthesias (Kuncel et al. 2008). Leads placed too medially are known to elicit intraoral paresthesias with stimulation, while paresthesias in the leg usually indicate that the lead is positioned too lateral. Furthermore, a 2 mm difference in electrode placement as compared to intended target identified through MR imaging has been reported in DBS procedures guided with intraoperative microelectrode recording

(MER) (McClelland et al. 2005). Given these anatomical constraints and the potential for slight targeting errors with neurosurgical implantation of the device, there is a strong need for developing DBS leads that will allow clinicians to more precisely modulate the neural pathways in and around thalamus in patients with ET.

In this study, we have developed a patient-specific computational modeling framework by which to evaluate a novel directionally segmented DBS lead for improving the overall therapeutic outcome. A segmented lead design would be beneficial for those patients whose DBS leads were inadvertently placed near Vc thalamus. Patient-specific thalamic models allowed us to compare 1) the clinical improvement in tremor to model predictions of the percentage of Vim afferent and efferent projections modulated during DBS as well as 2) the emergence of paresthesias to model predictions of the proportion of Vc afferent and efferent projections modulated during DBS.

Materials and Methods

Human Subjects

This study included retrospective computational modeling and image analysis of three patients who had been clinically diagnosed with essential tremor and who had been implanted with DBS lead(s) to suppress their upper extremity tremor symptoms (Table 1). Two patients had been implanted with unilateral left DBS implants, while the third patient received bilateral DBS implants (Medtronic 3389 leads). Imaging and clinical DBS programming data were de-identified prior to analysis.

Table 1: Subject Demographics

				Final DBS Setting				
Subject	**Age**	**Gender**	**Implant Side**	**Cathode**	**Anode**	**Pulse Width**	**Voltage**	**Frequency**
1	68	M	Left	2	Case	90 μs	2 V	185 Hz
2	76	M	Left	2	Case	90 μs	1 V	185 Hz
3	75	M	Left	1	Case	90 μs	2 V	185 Hz
			Right	2	3	90 μs	2.5 V	185 Hz

Anatomical Surface Reconstructions

Patient-specific computational models of the neuronal pathways affected by DBS were created for each subject. Pre-operative volumetric MR images were first aligned in Talairach coordinate space. Coronal MR slices containing thalamus were then matched to corresponding slices within the Mai human brain atlas (Mai et al. 2008). Because the clinical MRI resolution obtained from a 3T magnet had insufficient contrast to segment subnuclei within thalamus, a composite imaging and warped brain atlas approach was undertaken. Using a series of anatomically relevant landmarks, each brain atlas image was warped to conform to the patient MR slice using the software, Edgewarp 3.30 (Figure 1 A-B). Appendix 1 illustrates iterations of the warping process using various amounts of control points and the effect control point number had on the warped atlas result. This warping protocol was based off the methods used in a computational modeling study in the context of DBS of the STN and Lenticular Fasciculus (Miocinovic et al. 2006). The warped brain atlas images were then traced in Rhinoceros, a non-uniform rational basis spline program, to create a series of planar contours, each containing estimates of the anatomical borders of thalamic subnuclei including Vim and Vc. These contours were then lofted in three dimensions to create surface renderings of each thalamic nucleus. DBS leads were localized within the computational model space by co-registering post-operative CT images to the pre-operative MR images using the software Analyze (Figure 1 C).

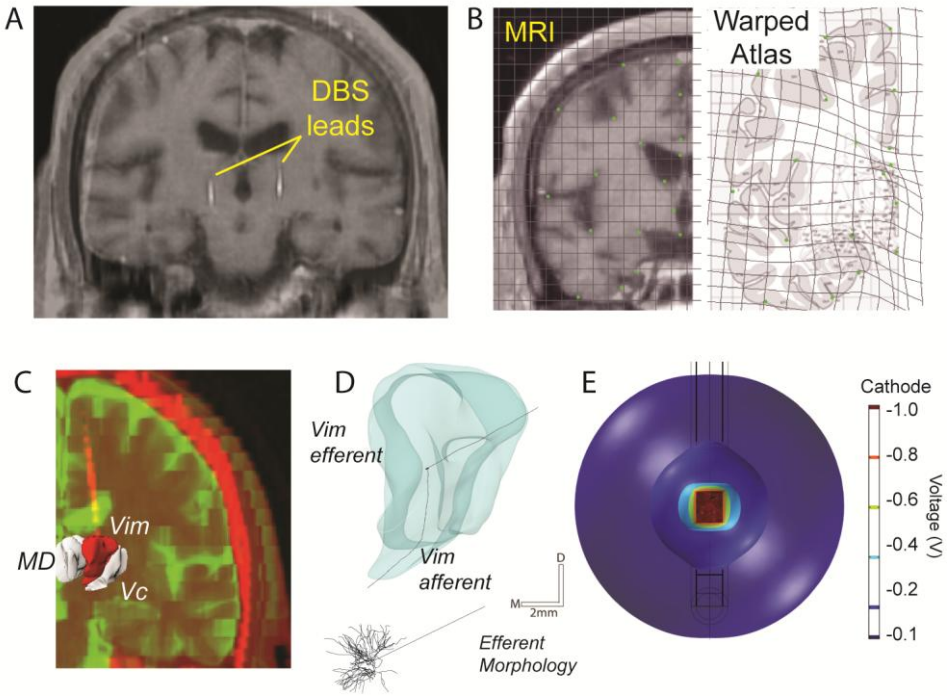

Figure 1: Patient-specific DBS modeling process. a) MR data for each patient was matched to the corresponding Mai atlas slice based on anatomical landmarks. b) Warping of a human brain atlas to MR images from each subject. c) Segmentation and co-registration of MRI and CT data for lead location. Tracing, aligning, and lofting of thalamic subnuclei. d) Each thalamic subnuclei contained multi-compartment model neurons and afferent axons. e) Finite element analysis simulating the voltage distribution in the brain during DBS.

Thalamic Neuron Morphologies and Projections

Vim and Vc thalamic volumes were populated with a neuron template consisting of an anatomically realistic, 3-D multi-compartment cable model of a thalamocortical (TC) relay cell (Figure 1 D). Because no study to date has reconstructed the full 3-D morphology of a TC neuron from the human brain, the TC relay cell model used in our study was given a dendritic morphology consistent with a previously published camera lucida reconstruction of a rodent TC cell (Destexhe et al. 1998). Though the cell reconstruction was from a rodent brain, the cell morphology and spread of the dendritic tree was within the range of cells reported from primate thalamus (Jones 2007). Previous non-human primate histological studies have shown that Vim thalamocortical neurons project to primary motor cortex (Hoover and Strick 1999), while Vc thalamocortical relay neurons terminate in the somatosensory cortex (Darian-Smith et al. 1999; Kultas-Ilinsky

et al. 2003). We modeled these thalamocortical efferent projections from reconstructions of biotinylated dextrane amine labeled neurons to the macaque motor cortex and subsequent 3-D reconstruction methods (Darian-Smith et al. 1999). The efferent path to cortex coursed along a medial-ventral to lateral-dorsal angle in the coronal plane and posterior-ventral to anterior-dorsal angle in the sagittal plane (Kakei et al. 2001). For the purpose of this study, the same neuron orientation was used for both Vim and Vc efferent neurons given the parallel anterior-posterior relationship between their cortical targets (Mai et al. 2008). This projection pattern is illustrated in Appendix 2. Five hundred copies of the neuron template were randomly distributed within both Vim and within Vc, allowing for a 10 degree randomized angle along both coronal and sagittal planes.

Cerebellothalamic tract afferents to Vim as well as lemniscal tract afferents to Vc were also reconstructed with multi-compartment cable model implementations. These tracts were based on the warped brain atlas from each patient with fibers coursing at an angle of approximately 45° with the intercommissural plane in the coronal plane. In the sagittal plane, the entrance to Vim and Vc thalamus followed a 60° angle with the intercommissural plane (Gallay et al. 2008). The axonal afferent models consisted of identical membrane properties and neuronal compartment lengths as the axon model of the efferents. The reconstructions (n=500) were populated along each tract with the distal end of each axon coinciding with a different neuron within Vim or Vc. There were two template afferent models distinguished by length; those in the top half of each thalamic nucleus were associated with longer afferents while those in the lower half of each thalamic nucleus were associated with shorter afferents. This categorization allowed the fiber tract entrance to the thalamus to remain anatomically confined to each patient's warped brain atlas.

Predicting Neuronal Responses to DBS

The Vim and Vc efferents and afferents were simulated within NEURON v7.1 programming environment (Hines and Carnevale 2009). Somatic and dendritic membrane properties were consistent with those defined previously (Destexhe et al. 1998; McIntyre et al. 2004) and included membrane capacitance, linear leakage properties, and nonlinear calcium, sodium, and potassium conductances. Axonal

processes consisted of nodes of Ranvier, myelin attachment segments, paranode main segments, and internode segments (Johnson and McIntyre 2008; McIntyre et al. 2004). Vim and Vc afferents were modeled as only axonal processes given the large distance between the stimulation source and the afferent cell bodies.

A 3-D finite element model (FEM) consisting of a tetrahedral mesh was modeled around each DBS lead using COMSOL Multiphysics v4.0 (Figure 1 E). The electric potential in the neural tissue surrounding the lead was modeled within a cylinder of radius 50 mm and height 50 mm with the outer bound set to ground potential, corresponding to a distant implantable pulse generator. The tissue surrounding the lead was modeled as a homogenous and isotropic medium with a conductivity of 0.3 S/m, except for an encapsulation layer at the electrode interface, which was represented by a 0.25 mm thick layer at 0.18 S/m. (Grill and Mortimer 1994; Haberler et al. 2000; Moss et al. 2004). The model assumed ideal electrode behavior and linear scaling of electric fields (Johnson and McIntyre 2008). The FEM model was solved with the frontal solution of the Laplace equation. Each compartment of each neuronal process was instantiated with a dynamic extracellular membrane potential consistent with the stimulation waveform and scaled according to the FEM solution.

Directionally-Segmented Lead Stimulation Calibration

The patient-specific neuronal models of DBS provided a method for comparing spatial activation profiles using a clinical DBS lead with four cylindrical contacts (Medtronic, 3389) to a novel DBS lead with directionally-oriented contacts (dDBS) (Martens et al. 2011). The dDBS lead investigated in this study was vertically as well as horizontally segmented and capable of shifting the spatial activation profile within the brain with sub-millimeter precision. This lead consisted of 16 equally spaced rows with 4 electrode contacts spanning each row (Figure 2). Each annular contact had a diameter of 0.5 mm and spacing between rows of 0.25 mm. The diameter of this lead design was 1.27 mm, matching the diameter of the Medtronic 3389 lead (Martens et al. 2011). In contrast to the voltage-controlled stimulation delivered through the 3389 DBS lead in the three Essential tremor subjects, the dDBS lead was simulated using current-controlled stimulation.

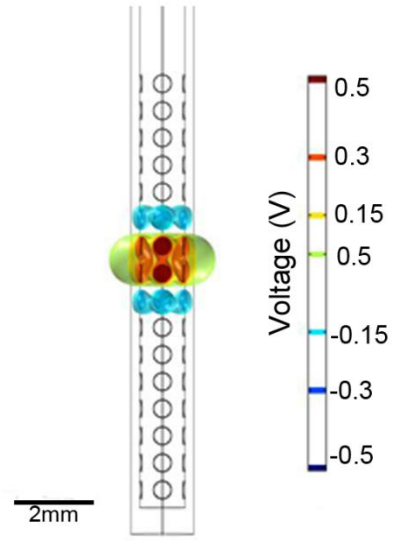

Figure 2: dDBS Lead Design. Example configuration illustration showing 8 cathodic contacts with two sets of 4 anodic contacts surrounding the two cathodic rows

In order to facilitate a comparison between cylindrical lead stimulation and dDBS lead stimulation, calibration between voltage and current sources was performed (Figure 3). It was assumed that electric field due to current stimulation scaled linearly as it was assumed for voltage-controlled stimulation. First, the electric potential surrounding a 1 V source applied to one of the cylindrical electrode contacts was modeled. This voltage distribution was compared to that produced with a variable current source using a test matrix of 400 points extending 9.5 mm horizontally and 9.5 mm vertically from the bounds of the distal contact. The current source magnitude was varied until the mean absolute error between the voltage source electric potential and the current source electric potential across the test matrix was minimized. A 2 mA current source produced the lowest mean error between the electric field distributions. An equivalent voltage distribution in the surrounding tissue to stimulation through a cylindrical contact was found to result from stimulating through 2 rows of contacts with the dDBS lead. In this case, the current source was divided between 8 contacts, yielding a current per contact of 0.25 mA. The current injection through each contact was 0.029 mC/cm^2 at the peak of stimulation (assuming 90 μs-long cathodic pulse), which was within the safe charge density limits (Shannon 1992).

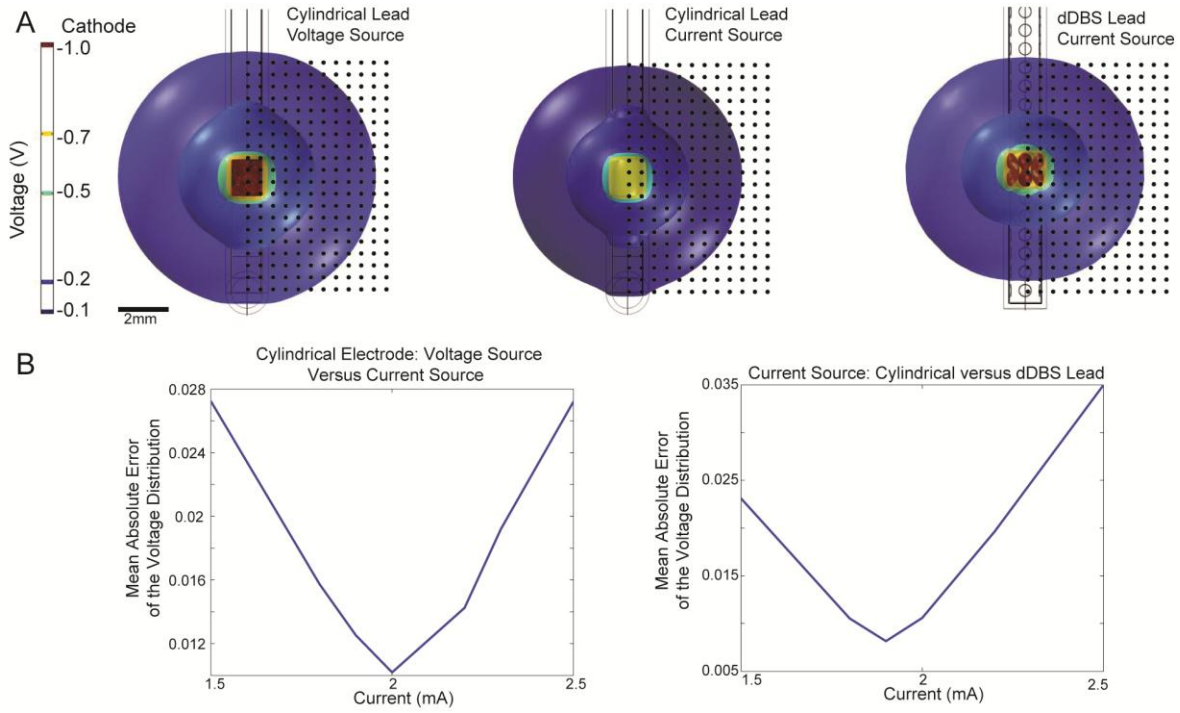

Figure 3: Calibration between voltage stimulation through the cylindrical lead and current stimulation through the dDBS lead. a) The conversion between voltage stimulation through the cylindrical lead and current stimulation through the segmented lead. The electric potential isosurfaces for the standard lead voltage source, current source, and dDBS lead current source are illustrated. A spatial sampling matrix was used to compare the voltage distribution surrounding the electrode contacts. b) Plots of mean error of the voltage distribution between the cylindrical lead- voltage source versus current source and for the cylindrical lead versus the dDBS lead using current controlled stimulation.

Stimulation Protocol

The stimulus pulse train was consistent with the implantable pulse generator (IPG) setting for each patient (185 Hz, 90 µs cathodic stimulus). The voltage waveform was based on experimental records of a voltage-controlled IPG (Medtronic, Minneapolis, MN), which exhibited a 90 µs cathodic pulse followed by a 400 µs interphase delay and a 3 ms anodic pulse. The signal was filtered in order to account for electrode-tissue capacitive properties (Butson and McIntyre 2005). In the case of current-controlled stimulation through the dDBS lead, the stimulus waveform was scaled from an

experimental recording of a constant-current IPG, matching the frequency and pulse-width implemented during clinical programming (Lempka et al. 2010).

Data Analysis

The data set included four DBS leads with a total of 50 stimulation parameter sets tested for tremor suppression efficacy and side-effect persistence. Clinical outcome to each of these setting was noted, and the outcomes of interest were grouped into one of four categories: incomplete improvement (n=4), complete improvement (n=10, 3 of 4 leads), transient paresthesias (n=5), and persistent paresthesias (n=12). Stimulation through Lead 4 was not able to sufficiently suppress tremor in Subject 3; therefore the outcomes form this lead were not included in this grouped data analysis. The remaining outcomes, including the report of no improvement and/or no-side effect, were those not statistically analyzed. The reader is referred to Appendix 3 for the neuronal activation profile for each lead.

The statistical tests employed were non-parametric given that the data was from a small sample size, and it was not normally distributed. In order to compare the continuous response variable, the percent neuronal activation, to the categorical treatment effect, the two-sided Mann-Whitney U test was performed at a significance level $p<0.05$. This non-parametric approach is used to test whether samples are drawn from the same distribution and have equal medians based on a rank comparison of the data. Because each response variable, or cell type, was treated as an independent sample, tests were performed separately and not corrected for multiple comparisons. Furthermore, the treatment effect was assumed to be binomial as the first set of data analyzed demonstrated incomplete or complete improvement in tremor, and the second set of data demonstrated either transient paresthesias or persistent paresthesias.

Results

Patient-Specific Modeling Predictions

The computational model predictions for activation of Vim/Vc efferents and afferents were compared with clinical outcome scores for the three lead implants that could achieve complete suppression of tremor (Figure 4). According to these

simulations, driving the output of Vim was associated with improved therapeutic benefit while Vc activation was associated with paresthesias. However, the mean percent activation in both efferent populations was low (8.7% and 9.9%, respectively). Including Vim and Vc afferents into the model was necessary to account for the improvement in tremor and onset of paresthesias in all patients. Figure 5 illustrates the Vim-thalamic model for each lead in a coronal perspective as well as a sagittal perspective. As seen in this figure, there was considerable variability amongst the four lead placements. Consistent across all leads is that the lead is implanted with at least one contact below the ventral border of Vim. Complete suppression of tremor was associated with an average of 62.4% (n=10) of the Vim afferents activated by the stimulation, whereas persistent paresthesias were associated with 35.3% (n=12) activation of Vc afferents.

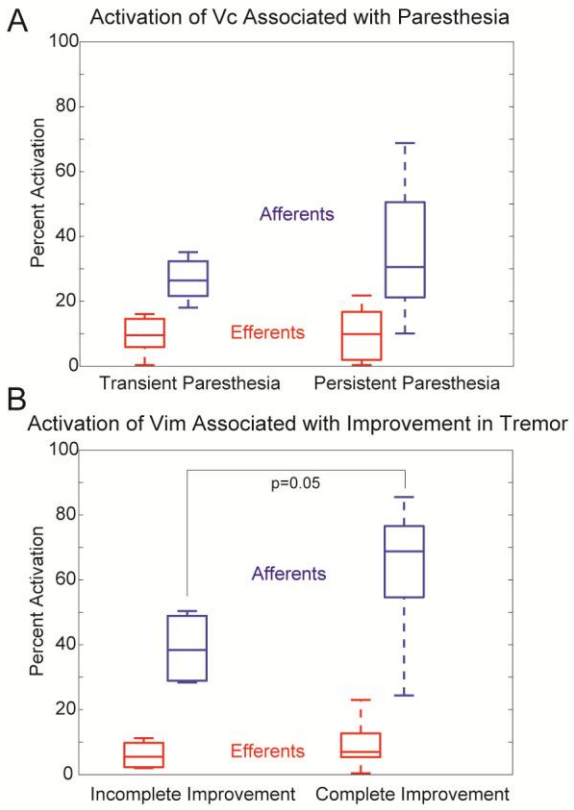

Figure 4: Neuronal activation of thalamic nuclei efferents and projecting axons eliciting side-effects or therapeutic benefit. a) Percent activation of Vc efferent and afferent projections for outcomes containing transient and persistent paresthesias (n=5, 12 outcomes). b) Percent activation of Vim efferent and afferent projections for outcomes containing incomplete and complete resolution of tremor (n=4, 10 outcomes).

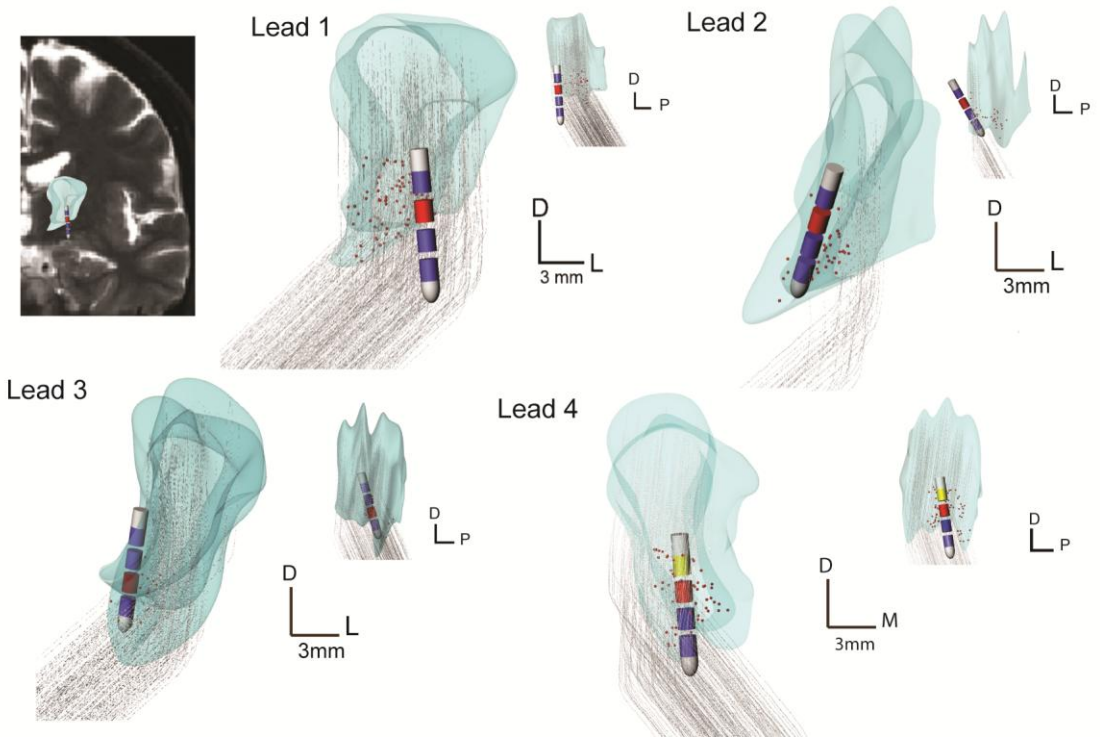

Figure 5: Patient-specific models illustrated for each subject. The MR image includes the Vim-thalamic volume of subject 1 and lead position. The images for each lead are patient-specific Vim volumes in a coronal and sagittal planes. Each illustrates DBS lead position and active contacts (cathode in red, anode in yellow, IPG was anode where not shown). Activated Vim neurons (indicated in red) and activated Vim afferents (pathways in gray) are also shown. Each representation is that of the clinical DBS setting that resulted in the clinician-identified best therapy. All scale bars are 3mm.

Non-parametric significance tests were performed to compare the median and distribution of neuronal activation looking at the effect of either suppression of tremor or emergence of paresthesias. The null hypothesis was that the data came from the same distribution with equal medians. In comparing the data from incomplete to complete resolution of tremor, the Vim afferents demonstrated a nearly statistical significance ($p=0.05$), while the Vim efferents did not reach significance ($p=0.52$). There was not a statistically significant difference for the progression from transient to persistent paresthesias for the Vc efferents ($p=0.96$) or Vc afferents ($p=0.57$). Therefore, the null hypothesis cannot be rejected in favor of the alternative that the median and distribution of the neuronal activation differed based on treatment outcome. It should be noted that

the follow up study will provide adequate sample sizes (n = 45 DBS leads) to support stronger statistical inferences.

Sensitivity Analysis of Lead Placement

Sensitivity to lead placement was evaluated by simulating DBS in the patient-specific models in which the lead was shifted 1 mm in one of four directions about the plane of the neurosurgical microdrive. This analysis was performed using each subject's final clinical DBS amplitude and waveform settings. The coordinates of the DBS lead were translated in a positive x and y, and negative x and y direction as shown in Figure 6. The largest variability in activation was found for the right implant in Subject 3 (Lead 4), in which incomplete suppression of tremor was achieved due to the emergence of paresthesias with increasing stimulation amplitude. In this case, neuronal activation ranged from 0.6% to 9.5% for Vc efferents, 7.5% to 38.9% for Vc afferents, from 17.2% to 21% for Vim efferents, and 67% to 92% for Vim afferents. These results indicate that for leads placed near the border of Vc, there is a high likelihood that onset of persistent paresthesias may occur at a DBS threshold below that for complete suppression of tremor. The lowest variability was observed for the implant in Subject 1 (Lead 1), in which the patient demonstrated complete resolution of tremor at only 1 V. For lead 1, the neuronal activation ranged from 13% to 19% for Vc efferents, 15% to 21% for Vc afferents, from 17% to 21% for Vim efferents, and 12% to 18% for Vim afferents. Leads 2 and 3 demonstrated neuronal activation variability between the extreme variability observed in 4 and the low variability of Lead 1.

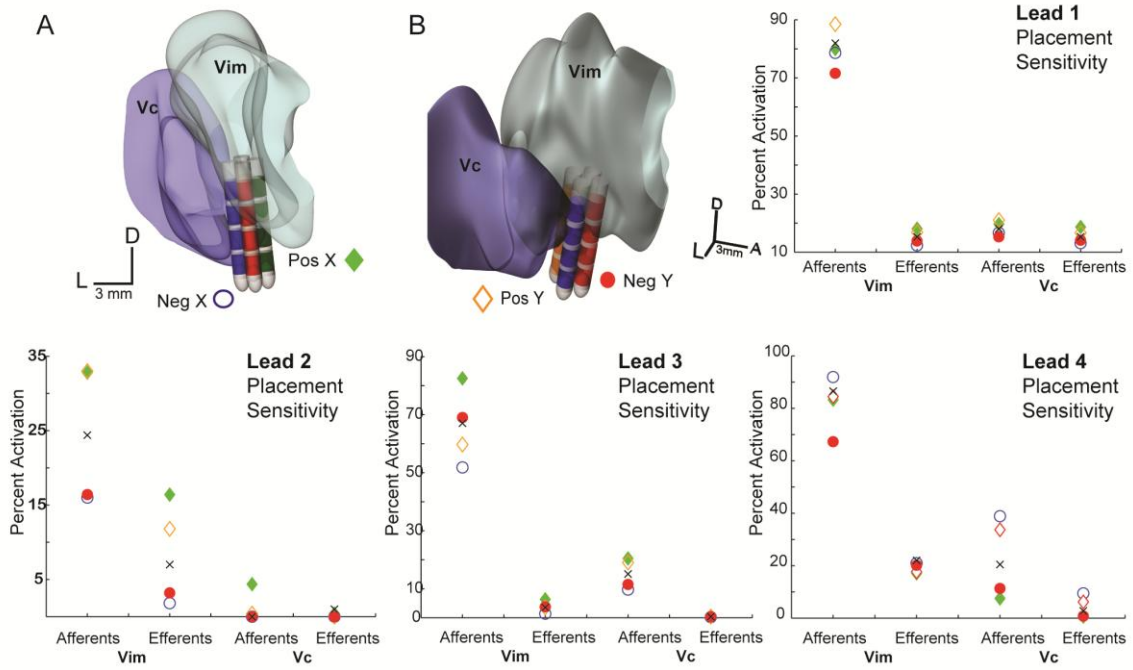

Figure 6: Sensitivity analysis of lead placement. This was performed by shifting the DBS lead 1 mm in each direction of the stereotactic microdrive plane. This displacement is illustrated in (a) and (b) for Subject 3, Lead 4. Each color is associated with a 1 mm shift in one direction (blue-negative x, green-positive x, orange-positive y, red- negative y). The x indicates the final clinical setting neuronal activation. Activation plots include the relative shift in each direction for each neuronal population plotted along the x-axis.

Novel Lead Performance

While three of the DBS implants in this study were able to completely suppress contralateral tremor, there was one case where DBS programming only achieved minimal benefit due to the emergence of persistent paresthesias with increasing stimulation amplitude. The DBS lead for this patient was programmed for bipolar stimulation in order to limit the volume of tissue activated surrounding the DBS lead; however, the therapeutic benefit on tremor remained less than optimal. This presented an interesting case to evaluate the directionally segmented lead performance in comparison to the standard lead performance. The computational models provided an opportunity to investigate if better therapy could have been achieved if the dDBS lead was implanted instead of the standard cylindrical electrode design (Figure 7).

Five dDBS stimulation configurations were evaluated in terms of their ability to target the cerebello-thalamo-cortical pathway (Vim afferents and efferents) without concurrent activation of Vc thalamus. For each of the five dDBS electrode configurations evaluated, a current balance was maintained. The first model (Model A) was designed to closely match the patient's final bipolar electrode configuration through a Medtronic 3389 lead. However, it should be noted that there was still a discrepancy between the modeled neuronal activation for the final voltage-controlled bipolar stimulation implemented in the clinic and the dDBS lead configuration. The dDBS electrode configuration consisted of two rows of cathodic contacts and two rows of anodic contacts, matching the locations of the cathode and anode of the clinical cylindrical lead. Models B-E used an 8-contact cathode arrangement of four rows and two adjacent electrode contacts oriented toward the Vim. Models B and D were designed to have the cathodic contacts facing Vim and the anodic contacts oriented in the opposite direction towards Vc, given the higher activation volumes with cathodic stimulation (McIntyre and Grill 2002). While Model B demonstrated a balanced number of cathodic contacts and anodic contacts, Model D was configured to have 16 anodic contacts but still maintained an equal balance of cathodic and anodic current amplitude. Models C and E were designed to have the cathode surrounded vertically by anodes, all of which faced towards Vim. Again, Model C had a configuration with 8 anodic contacts whereas Model E had 16 anodic contacts with equal current stimulation through cathode and anode. These settings were chosen to demonstrate the capability of the segmented lead to activate pathways with fine adjustment based on the individual contact settings.

The results shown in Figure 7 suggest that a more desirable stimulation protocol could be implemented using Model D rather than the cylindrical DBS lead implanted in practice. Model A was configured to closely match the stimulation settings of the clinical bipolar case. As seen in Figure 7, Model A demonstrated Vim efferent activation lower than all of the other models, and the Vc efferent activation was higher than all the other models. On the other hand, Model D demonstrates a case where Vim efferent activation is high, and Vc efferent activation is low. While Model D does not demonstrate the highest Vim afferent percent activation associated with each current setting, the response profile does fall between the other models. Additionally, at a 6 mA current injection,

which is equivalent to a 3 V stimulation, the neuronal activation of Vim afferents is 60.2%. According to the modeling results presented in this study, this stimulation setting would likely result in complete resolution of tremor. Moreover, the Vc afferent activation profile is lower throughout all current stimulation settings as compared to the other models simulated in this design. In practice, more complex settings could be applied in order to achieve optimal therapy.

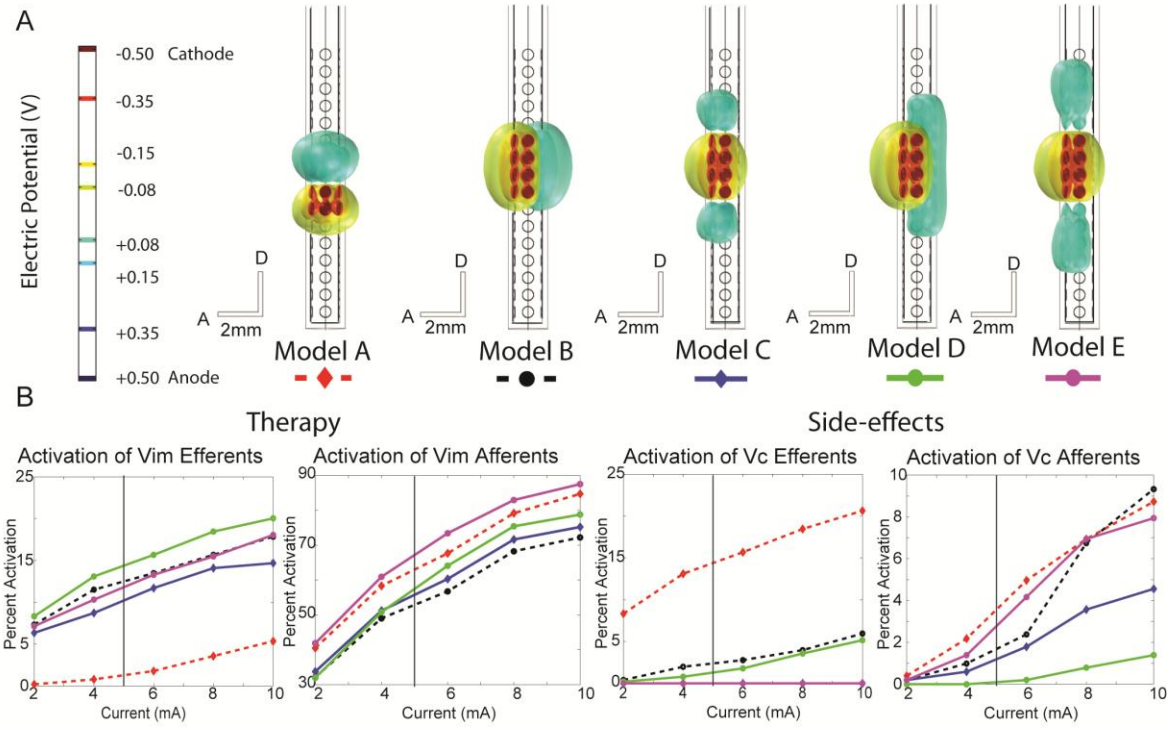

Figure 7: Five dDBS stimulation configurations and associated activation profiles. Five dDBS models were evaluated in place of the cylindrical lead for the right implant in Subject 3, which never achieved optimal therapeutic effects. a) dDBS lead configurations with isosurfaces illustrating electric potential voltage surrounding the lead. Cathodic contacts are indicated in red and anodic contacts in blue. Model A represents a close match between the dDBS lead and the bipolar setting finalized in the clinic. Models B-E maintained eight cathodic contacts oriented towards the Vim while the anodic contacts were shifted around the lead for assessment of optimized activation. The Vim is located anterior to the lead, and the Vc is located posterior to the lead. b) Activation plots of Vim and Vc efferents and afferents versus total current injection. The vertical bar represents the equivalent voltage source stimulated in the final clinical setting.

Discussion

This study provided a framework by which to quantify the neuronal pathways modulated during DBS for ET. The models support the hypothesis that driving afferents into Vim is a possible mechanism for the resolution of tremor with DBS, as recently hypothesized through a network model (Birdno et al. 2011). Furthermore, our models provided a patient-specific framework by which to evaluate the novel DBS lead design aimed at steering current toward those pathways involved in the therapeutic mechanisms of action and away from those associated with side effects.

Model Calibration

Calibration of computational models of DBS has been previously achieved by coupling predictions of internal capsule stimulation with EMG recordings of distal muscle groups (Butson et al. 2011). In this study, we defined a calibration method by correlating induction of transient and persistent paresthesias with activation of the axonal afferents into and efferents out of Vc thalamus. DBS in and near the Vc is known to cause somatic sensations, as receptive fields are localized within Vc that respond to sensory stimulation (Hua et al. 2000). High frequency stimulation of Vc has been linked to eliciting paresthesias (Kuncel et al. 2008). The model that we present demonstrated that an activation of 9.9% Vc efferents, on average (n=12), was associated with persistent paresthesias.

It should be noted that absolute percentages and the underlying neuronal excitability they represent depend on a variety of model parameter assumptions. The model thalamocortical neuron template (Destexhe et al. 1998), and the afferent axons coinciding with each, may not fully represent the dynamics and morphologies present in the human brain of Essential Tremor patients. Furthermore, the model assumes the brain tissue behaves as an isotropic medium outside of the encapsulation layer. In order to account for diverse tissue properties, an anisotropic conductance model of the brain could be constructed using diffusion tensor imaging (DTI) for each patient, which was outside the scope of the current study. Additionally, due to insufficient resolution in the patient imaging data, the reconstruction of the thalamus was carried out by warping a human

brain atlas to the patient MRI instead of a direct segmentation from the MRI. Future work utilizing high-field (7T) MRI will provide a means to segment individual subnuclei within thalamus (Abosch et al. 2010) and enable high-resolution tractography through diffusion tensor imaging (Tournier et al. 2011). High-resolution tractography for each patient may potentially allow for more anatomically realistic placement and orientation of the cerebellothalamic fibers and medial lemniscal fibers entering the thalamic nuclei on a patient-specific basis. As targeting the cerebellothalamic tract increases in popularity as a viable alternative to targeting the Vim proper, such techniques could enhance the therapeutic benefit due to stimulation.

The measure of treatment outcome in this study was based on the clinician's subjective assessment of tremor rating and the patient's subjective reporting of paresthesias when they occurred. Both of these factors likely contributed to the variability among model predictions. A treatment effect quantified as a discrete ordinal variable would be advantageous in assessing stimulation effect. While this limitation cannot be disregarded from the model results, a follow-up study with a larger sample size may help to better account for such variability.

Additionally, since the leads in this study tended to be placed in the ventral portion of Vim with at least one contact extending beyond the ventral border of the Vim, it is possible that the model was biased in favor of supporting the claim that activation of the afferent projections into thalamus rather than the efferent output drive therapeutic outcome. Therefore, we do not conclude that this cerebellothalamic tract stimulation is superior to efferent activation, although it has been suggested through imaging studies localizing the position of the most therapeutic electrode contacts relative to Vim (Sandvik et al. 2011). Our results present evidence that stimulation of the cerebellothalamic tract is a viable explanation for the mechanisms of tremor reduction; however, other fiber tracts may also be present within the volume of activation including pallidothalamic fibers, zona incerta projections, and other tract passing to and from midbrain and brainstem nuclei (Baron et al. 2001; Blomstedt et al. 2009; Gallay et al. 2008).

Cerebellothalamic Tract Stimulation

The optimal lead placement to alleviate tremor with the lowest stimulation energy

requirements remains a matter of debate. Across the four DBS lead implants in this study, suppression of tremor was associated with a greater activation of Vim afferent fibers than Vim efferent neurons, due in part to the deep placement of the lead with respect to Vim. Stimulation below the AC-PC plane has been shown to be more efficient than stimulation above the AC-PC plane (Sandvik et al. 2011), which is consistent with the model predictions showing greater activation of cerebellothalamic tract fibers with increasing improvement in tremor suppression. Because the cerebellothalamic tract has a cross-sectional area significantly smaller than that of Vim, the volume of tissue to modulate a significant portion of Vim may be smaller for DBS leads located within the cerebellothalamic tract (Hirai et al. 1983). Using two leads in cases of Vim-DBS was shown to provide greater therapeutic benefit, potentially by affecting a greater area of the thalamus during stimulation (Foote and Okun 2005; Kobayashi et al. 2010).

Others have argued that the optimal target of DBS for ET is within the Vim. (Benabid et al. 1991; Kobayashi et al. 2010). This target presents a challenge for implantation as displacements in ideal trajectories on the millimeter scale may result in poor resolution of tremor and production of disabling side-effects. The sensitivity analysis shown in our study demonstrates the importance of precise implantation as millimeter shifts in lead placement lead to large variations in neuronal activation of both Vim and Vc. These results suggest that although the nucleus may be an effective location for stimulation, the standard cylindrical lead may not suffice in effectively activating the proper neuronal processes. As such we investigated the feasibility of using a directionally segmented lead design to enable more effective therapy without inducing paresthesias.

Directionally-Segmented DBS Leads

The primary advantage of a lead design such as the dDBS lead is the capacity to tailor the effects of stimulation more precisely within the brain with sub-millimeter precision (Martens et al. 2011). This type of accuracy is desirable when the lead is implanted near the Vim/Vc border. Such was the case for the right implant in Subject 3. The computational models developed in this study suggest that stimulating through the dDBS lead rather than the standard cylindrical configuration would have led to a better

suppression of symptoms. This can be deduced by comparing the activation plots in Figure 7 from Model A, representative of the clinical bipolar setting, and Model D. Similar benefits would likely be achieved in other small and anatomically complex target regions where directed current steering is desirable, such as in the subthalamic nucleus (STN) or the pedunculopontine nucleus (PPN). Indeed, it has been reported for one DBS clinic that for implants targeting STN, the targeting error between intended DBS location and actual DBS location was 2 mm (McClelland et al. 2005).

The Medtronic 3387 DBS lead has four 1.5 mm contacts with spacing in between contacts of 1.5 mm. Medtronic 3389 DBS leads have four 1.5mm contacts with spacing between contacts of 0.5 mm. The contacts for both leads are numbered 0, 1, 2, and 3 in a distal to proximal fashion when the lead is implanted. The leads implanted in this study were 3389 leads, meaning the contacts spanned a space of 7.5 mm whereas the Medtronic 3387 leads span a space of 10.5mm. Three of the four final clinical settings were monopoloar configurations with stimulating electrodes at contact 1 or 2. In these cases, the standard 3389 lead was sufficient to capture good tremor resolution. However, one of the DBS leads was not able to completely resolve tremor, and a bipolar stimulation approach was used with the cathode at contact 2 and the anode at contact 3. The dDBS lead, which spans a space of 15.5 mm, would enable the clinician to stimulate through more dorsal contacts if desirable. While such stimulation may activate additional Vim afferents and efferents such dDBS configurations were not assessed as part of this study.

Moreover, the effect of contact geometry on the volume of tissue activated is an important consideration to keep in mind when developing a new DBS lead design. It was previously reported that the shape of the volume of tissue activated is influenced by electrode diameter and height (Butson and McIntyre 2006). The results from their study suggest that electrodes with a low ratio between diameter and height would best maximize the volume of tissue activated (Butson and McIntyre 2006). In this study, the dDBS lead design had the same diameter as the standard Medtronic lead (1.27mm), however, the height of the contact was decreased to 0.5mm. Because of this, the volume of tissue activated by each contact is lower than what would be activated through the standard DBS lead. While the voltage of tissue activated per contacts is lower, a potential benefit to using smaller contact sizes arises if the DBS target is located adjacent

to neuronal tissue associated with side-effects (Vim). The dDBS lead design would provide possible stimulation paradigms that could shape the volume of tissue activated towards the therapeutic target and away from the adjacent structures.

In addition to considering the contact's geometry on the volume of tissue activated, it is important to keep in mind the safety parameters of neural stimulation in mind. The proposed dDBS lead design has a small contact size ($0.195mm^2$) as compared to the Medtronic 3389 contact size ($6mm^2$). This, in turn, means that the charge density at the electrode surface would be higher in the dDBS lead than in the 3389 Medtronic lead at the same stimulus level. However, for this study, the maximum current injection through the dDBS lead was 10mA, and the maximum current density per contact was $29\mu C/cm^2$, which has been suggested as the limit for safe charge injection (Shannon 1992). Furthermore, in future evaluations of dDBS lead stimulation paradigms, the current restrictions governing safe stimulation must be taken into account.

Finally, for some patients, the beneficial effects of Vim-DBS have been observed to gradually decrease with time (Barbe et al. 2011b; Benabid et al. 1996; Blomstedt et al. 2007). Clinicians may choose to increase stimulation amplitude, which may lead to side-effects. There was also a report of implanting a second parallel lead in an attempt to arrest the tremor (Yu et al. 2009). Alternatively, stimulation with the dDBS lead explored in this study could provide an efficient method to control the spread of the stimulation field to alternative pathways involved in the pathophysiology of Essential Tremor. Using patient-specific modeling in the clinic could provide a potential solution to this problem, as an optimal parameter set can first be chosen based on the models.

Future Directions

The aim of this study was to develop a patient-specific computational modeling framework in order to evaluate the efficacy of a novel lead design. The data set analyzed in this sample was too small to confidently draw conclusions regarding efficacy of stimulation parameters based on lead location and subsequent activation of neuronal population profiles. However, sampling from a larger distribution will allow us to test these relationships with a greater statistical power. Non-parametric statistical measures were used in this study to analyze the data. Non-parametric tests tend to give a

conservative association of variables as the data cannot be assumed to come from a normal distribution. The next step in this study will include analyzing 45 more DBS implants for patient's diagnosed with Essential tremor (30 subjects). The statistics collected from this larger data set will lend itself to statistical measures of greater power. Furthermore, a categorization of symptoms into more than one category should be considered such as when the patient is reported to demonstrate no resolution in tremor while simultaneously experiencing no side-effects.

In this study, the neuronal tissue activated was modeled as independent samples. In the future, associating the Vim afferents with Vim efferents and similarly linking Vc afferents with Vc efferents may be provide additional evidence and support for best lead placement and stimulation parameters. One possibility would be to include one or more synapses with appropriate synapse dynamics between the afferents and each efferent. An alternate method would be to develop a statistical method accounting for dependency between the afferent and efferent population dynamics. Furthermore, in order to enhance the model, it may be desirable to include a sample of characteristic burster cells. While the origin of the bursting activity is unknown, including this characteristic of TC tremor cells may enhance the model by making it more physiologically realistic. Both of these considerations were beyond the scope of this study but could be pursued in future analysis.

Finally, the evaluation of the dDBS lead in this study was limited to five lead configurations. The model configurations and stimulation settings were limited so that a reasonable comparison to the clinical bipolar setting could be assessed. The location and number of cathodic contacts remained the same thus limiting the variables influencing the neuronal activation profiles. In the future, an optimization algorithm determining the optimal dDBS configuration and stimulation setting should be developed. The first step in this process will be to sample data from a larger data set and determine statistical measures of treatment outcomes. These measures can then be used to assess the efficacy of stimulation configurations. Another factor that will need to be taken into account is stimulation efficacy. The aim will be to limit the current magnitude required to achieve optimal therapy while avoiding side-effects.

Although the dDBS lead may provide improved outcomes in patients with Essential Tremor, one of the potential challenges will be programming the stimulation settings of such a lead, especially if the patient was implanted with a neurostimulator capable of independent channel, current-controlled stimulation. In our study, only five dDBS lead settings are reported, though countless more could be assessed. Simplifying the DBS parameter space to a few electrode configurations will be an important next step for this type of lead to have a positive impact in the clinic. An optimization solution space will be necessary to take into account the efficacy of therapy against the current required for stimulation. A logical starting point for determining effective therapy will be to begin with a dDBS lead configuration closely matching the final standard lead stimulation configuration and build more complex electrode configurations from it.

Conclusion

This study illustrates instances in which postural and intentional tremor were resolved with stimulation through DBS leads placed near the ventral border of Vim. We found that the inclusion of Vim and Vc efferents alone were not sufficient to account for differences in observed outcomes. The inclusion of cerebellothalamic projections to the Vim thalamus along with medial lemniscal projections to the Vc thalamus were necessary to fit the model data to the clinical results. This finding complements previous studies suggesting Vim afferents may also be a target for relieving tremor (Herzog et al. 2007). Future work in identifying both the underlying pathways causing tremor activity as well as the localization of optimal DBS stimulation site(s) will continue to improve the positive outcomes demonstrated by those who undergo DBS for ET. While these pathways are being explored, it will be advantageous to continue to develop computational models for assessing the efficacy of new lead designs and also to test these leads in animals as they may lead to enhanced and more robust therapeutic outcomes. Further, the results from this computational modeling study suggest that for patients with leads positioned near Vc thalamus, a directionally segmented DBS lead design may allow clinicians to better target the cerebello-thalamo-cortical pathway without inducing unwanted side effects.

References

Abosch A, Yacoub E, Ugurbil K, and Harel N. An assessment of current brain targets for deep brain stimulation surgery with susceptibility-weighted imaging at 7 tesla. *Neurosurgery* 67: 1745-1756; discussion 1756, 2010.

Barbe MT, Liebhart L, Runge M, Deyng J, Florin E, Wojtecki L, Schnitzler A, Allert N, Sturm V, Fink GR, Maarouf M, and Timmermann L. Deep brain stimulation of the ventral intermediate nucleus in patients with essential tremor: stimulation below intercommissural line is more efficient but equally effective as stimulation above. *Experimental neurology* 230: 131-137, 2011a.

Barbe MT, Liebhart L, Runge M, Pauls KA, Wojtecki L, Schnitzler A, Allert N, Fink GR, Sturm V, Maarouf M, and Timmermann L. Deep brain stimulation in the nucleus ventralis intermedius in patients with essential tremor: habituation of tremor suppression. *Journal of neurology* 258: 434-439, 2011b.

Baron MS, Sidibe M, DeLong MR, and Smith Y. Course of motor and associative pallidothalamic projections in monkeys. *The Journal of comparative neurology* 429: 490-501, 2001.

Benabid AL, Lebas JF, Grand S, Benazzouz A, Pollak P, Krack P, Koudsie A, Chabardes S, Fraix V, Limousin P, Pinto S, Hoffmann D, Ardouin C, and Funkiewiez A. Deep brain stimulation for movement disorders. In: *Youmans Neurological Surgery*, edited by Winn HR. Philadelphia: Saunders, 2004.

Benabid AL, Pollak P, Gao D, Hoffmann D, Limousin P, Gay E, Payen I, and Benazzouz A. Chronic electrical stimulation of the ventralis intermedius nucleus of the thalamus as a treatment of movement disorders. *J Neurosurg* 84: 203-214, 1996.

Benabid AL, Pollak P, Gervason C, Hoffmann D, Gao DM, Hommel M, Perret JE, and de Rougemont J. Long-term suppression of tremor by chronic stimulation of the ventral intermediate thalamic nucleus. *Lancet* 337: 403-406, 1991.

Birdno MJ, Kuncel AM, Dorval AD, 2nd, Turner DA, Gross RE, and Grill WM. Stimulus features underlying reduced tremor suppression with temporally patterned deep brain stimulation. *J Neurophysiol* 2011.

Birdno MJ, Kuncel AM, Dorval AD, Turner DA, and Grill WM. Tremor varies as a function of the temporal regularity of deep brain stimulation. *Neuroreport* 19: 599-602, 2008.

Blomstedt P, Hariz GM, Hariz MI, and Koskinen LO. Thalamic deep brain stimulation in the treatment of essential tremor: a long-term follow-up. *British journal of neurosurgery* 21: 504-509, 2007.

Blomstedt P, Sandvik U, Fytagoridis A, and Tisch S. The Posterior Subthalamic Area in the Treatment of Movement Disorders: Past, Present, and Future. *Neurosurgery* 64: 1029-1038, 2009.

Butson CR, Cooper SE, Henderson JM, and McIntyre CC. Patient-specific analysis of the volume of tissue activated during deep brain stimulation. *NeuroImage* 34: 661-670, 2007.

Butson CR, Cooper SE, Henderson JM, Wolgamuth B, and McIntyre CC. Probabilistic analysis of activation volumes generated during deep brain stimulation. *NeuroImage* 54: 2096-2104, 2011.

Butson CR, and McIntyre CC. Role of electrode design on the volume of tissue activated during deep brain stimulation. *J Neural Eng* 3: 1-8, 2006.

Butson CR, and McIntyre CC. Tissue and electrode capacitance reduce neural activation volumes during deep brain stimulation. *Clinical neurophysiology : official journal of the International Federation of Clinical Neurophysiology* 116: 2490-2500, 2005.

Darian-Smith C, Tan A, and Edwards S. Comparing thalamocortical and corticothalamic microstructure and spatial reciprocity in the macaque ventral posterolateral nucleus (VPLc) and medial pulvinar. *The Journal of comparative neurology* 410: 211-234, 1999.

Destexhe A, Neubig M, Ulrich D, and Huguenard J. Dendritic low-threshold calcium currents in thalamic relay cells. *The Journal of neuroscience : the official journal of the Society for Neuroscience* 18: 3574-3588, 1998.

Foote KD, and Okun MS. Ventralis intermedius plus ventralis oralis anterior and posterior deep brain stimulation for posttraumatic Holmes tremor: two leads may be better than one: technical note. *Neurosurgery* 56: E445; discussion E445, 2005.

Gallay MN, Jeanmonod D, Liu J, and Morel A. Human pallidothalamic and cerebellothalamic tracts: anatomical basis for functional stereotactic neurosurgery. *Brain structure & function* 212: 443-463, 2008.

Grill WM, and Mortimer JT. Electrical properties of implant encapsulation tissue. *Annals of biomedical engineering* 22: 23-33, 1994.

Haberler C, Alesch F, Mazal PR, Pilz P, Jellinger K, Pinter MM, Hainfellner JA, and Budka H. No tissue damage by chronic deep brain stimulation in Parkinson's disease. *Annals of neurology* 48: 372-376, 2000.

Hallett M, and Dubinsky RM. Glucose metabolism in the brain of patients with essential tremor. *Journal of the neurological sciences* 114: 45-48, 1993.

Herzog J, Hamel W, Wenzelburger R, Potter M, Pinsker MO, Bartussek J, Morsnowski A, Steigerwald F, Deuschl G, and Volkmann J. Kinematic analysis of thalamic versus subthalamic neurostimulation in postural and intention tremor. *Brain* 130: 1608-1625, 2007.

Hirai T, Miyazaki M, Nakajima H, Shibazaki T, and Ohye C. The correlation between tremor characteristics and the predicted volume of effective lesions in stereotaxic nucleus ventralis intermedius thalamotomy. *Brain* 106 (Pt 4): 1001-1018, 1983.

Hoover JE, and Strick PL. The organization of cerebellar and basal ganglia outputs to primary motor cortex as revealed by retrograde transneuronal transport of herpes simplex virus type 1. *The Journal of neuroscience : the official journal of the Society for Neuroscience* 19: 1446-1463, 1999.

Hua SE, Garonzik IM, Lee JI, and Lenz FA. Microelectrode studies of normal organization and plasticity of human somatosensory thalamus. *J Clin Neurophysiol* 17: 559-574, 2000.

Hua SE, Lenz FA, Zirh TA, Reich SG, and Dougherty PM. Thalamic neuronal activity correlated with essential tremor. *Journal of neurology, neurosurgery, and psychiatry* 64: 273-276, 1998.

Jenkins IH, Bain PG, Colebatch JG, Thompson PD, Findley LJ, Frackowiak RS, Marsden CD, and Brooks DJ. A positron emission tomography study of essential

tremor: evidence for overactivity of cerebellar connections. *Annals of neurology* 34: 82-90, 1993.

Johnson MD, and McIntyre CC. Quantifying the neural elements activated and inhibited by globus pallidus deep brain stimulation. *J Neurophysiol* 100: 2549-2563, 2008.

Jones EG. *The thalamus*. Cambridge ; New York: Cambridge University Press, 2007.

Kakei S, Na J, and Shinoda Y. Thalamic terminal morphology and distribution of single corticothalamic axons originating from layers 5 and 6 of the cat motor cortex. *The Journal of comparative neurology* 437: 170-185, 2001.

Kobayashi K, Katayama Y, Sumi K, Otaka T, Obuchi T, Kano T, Nagaoka T, Oshima H, Fukaya C, Yamamoto T, and Atsumi H. Effects of electrode implantation angle on thalamic stimulation for treatment of tremor. *Neuromodulation : journal of the International Neuromodulation Society* 13: 31-36, 2010.

Kultas-Ilinsky K, Sivan-Loukianova E, and Ilinsky IA. Reevaluation of the primary motor cortex connections with the thalamus in primates. *The Journal of comparative neurology* 457: 133-158, 2003.

Kuncel AM, Cooper SE, and Grill WM. A method to estimate the spatial extent of activation in thalamic deep brain stimulation. *Clinical neurophysiology : official journal of the International Federation of Clinical Neurophysiology* 119: 2148-2158, 2008.

Lempka SF, Johnson MD, Miocinovic S, Vitek JL, and McIntyre CC. Current-controlled deep brain stimulation reduces in vivo voltage fluctuations observed during voltage-controlled stimulation. *Clinical neurophysiology : official journal of the International Federation of Clinical Neurophysiology* 121: 2128-2133, 2010.

Louis ED, Ottman R, and Hauser WA. How common is the most common adult movement disorder? estimates of the prevalence of essential tremor throughout the world. *Mov Disord* 13: 5-10, 1998.

Lozano AM. Vim thalamic stimulation for tremor. *Archives of medical research* 31: 266-269, 2000.

Mai JK, Paxinos G, and Voss T. *Atlas of the human brain*. New York: Academic Press, 2008.

Martens HC, Toader E, Decre MM, Anderson DJ, Vetter R, Kipke DR, Baker KB, Johnson MD, and Vitek JL. Spatial steering of deep brain stimulation volumes using a novel lead design. *Clinical neurophysiology : official journal of the International Federation of Clinical Neurophysiology* 122: 558-566, 2011.

McClelland S, 3rd, Ford B, Senatus PB, Winfield LM, Du YE, Pullman SL, Yu Q, Frucht SJ, McKhann GM, 2nd, and Goodman RR. Subthalamic stimulation for Parkinson disease: determination of electrode location necessary for clinical efficacy. *Neurosurg Focus* 19: E12, 2005.

McIntyre CC, and Grill WM. Extracellular stimulation of central neurons: influence of stimulus waveform and frequency on neuronal output. *J Neurophysiol* 88: 1592-1604, 2002.

McIntyre CC, Grill WM, Sherman DL, and Thakor NV. Cellular effects of deep brain stimulation: model-based analysis of activation and inhibition. *J Neurophysiol* 91: 1457-1469, 2004.

Miocinovic S, Parent M, Butson CR, Hahn PJ, Russo GS, Vitek JL, and McIntyre CC. Computational analysis of subthalamic nucleus and lenticular fasciculus activation during therapeutic deep brain stimulation. *J Neurophysiol* 96: 1569-1580, 2006.

Moss J, Ryder T, Aziz TZ, Graeber MB, and Bain PG. Electron microscopy of tissue adherent to explanted electrodes in dystonia and Parkinson's disease. *Brain* 127: 2755-2763, 2004.

Plaha P, Ben-Shlomo Y, Patel NK, and Gill SS. Stimulation of the caudal zona incerta is superior to stimulation of the subthalamic nucleus in improving contralateral parkinsonism. *Brain* 129: 1732-1747, 2006.

Sandvik U, Lars-Owe K, Anders L, and Patric B. Thalamic and subthalamic DBS for essential tremor: where is the optimal target? *Neurosurgery* 2011.

Shannon RV. A model of safe levels for electrical stimulation. *IEEE transactions on bio-medical engineering* 39: 424-426, 1992.

Sherman SM, and Guillery RW. Functional organization of thalamocortical relays. *J Neurophysiol* 76: 1367-1395, 1996.

Tournier JD, Mori S, and Leemans A. Diffusion Tensor Imaging and Beyond. *Magn Reson Med* 65: 1532-1556, 2011.

Whaley NR, Putzke JD, Baba Y, Wszolek ZK, and Uitti RJ. Essential tremor: phenotypic expression in a clinical cohort. *Parkinsonism Relat Disord* 13: 333-339, 2007.

Yu H, Hedera P, Fang J, Davis TL, and Konrad PE. Confined stimulation using dual thalamic deep brain stimulation leads rescues refractory essential tremor: report of three cases. *Stereotactic and functional neurosurgery* 87: 309-313, 2009.

Zesiewicz TA, Chari A, Jahan I, Miller AM, and Sullivan KL. Overview of essential tremor. *Neuropsychiatr Dis Treat* 6: 401-408, 2010.

Appendix 1:Warping Procedure

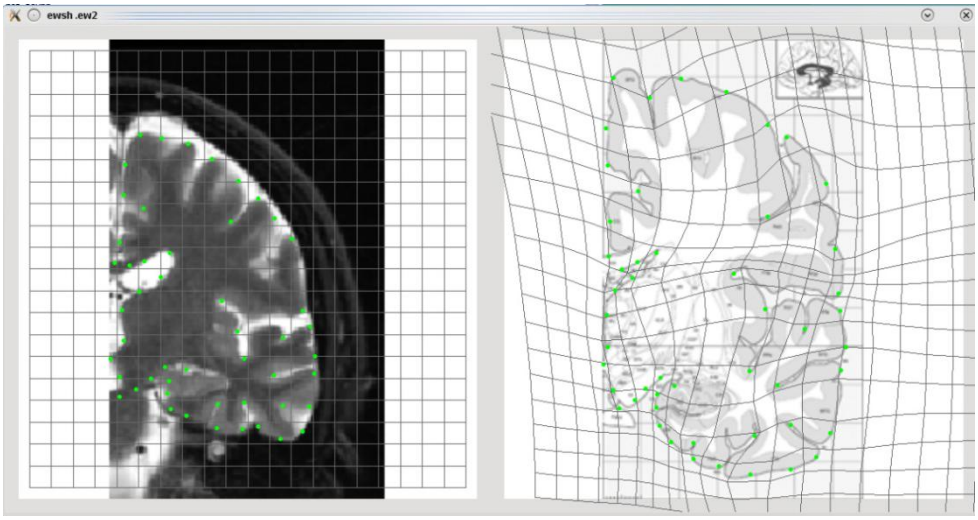

Figure 8: Edgewarp demonstration. The left image is of the patient MR data with control points in green, which are matched to the coinciding landmarks on the atlas page (right image) and warped using a Biometric

Figure 8 is a demonstration of patient MR data with control points (left) and warped atlas image (right) using the program Edgewarp 3.30 (Bookstein 1990). Below is a comparison of four warped images using different numbers of control points. Control points from left to right follow 25, 35, 45, and 50 control points. In this study, the control points used varied, but as seen in the figures, the number of control points used primarily influences the shape and structure of the cortical structure and does not shift the location or size of the thalamic nuclei considerably. For this reason, a control point range between 35 points and 45 points was used throughout the study. Note that when tracing the nuclei in the 3-D Rhino program, the corresponding intact brain atlas slice was used as a guide for correctly labeling nuclei as the labels are blurred in the warped images produced by Edgwarp.

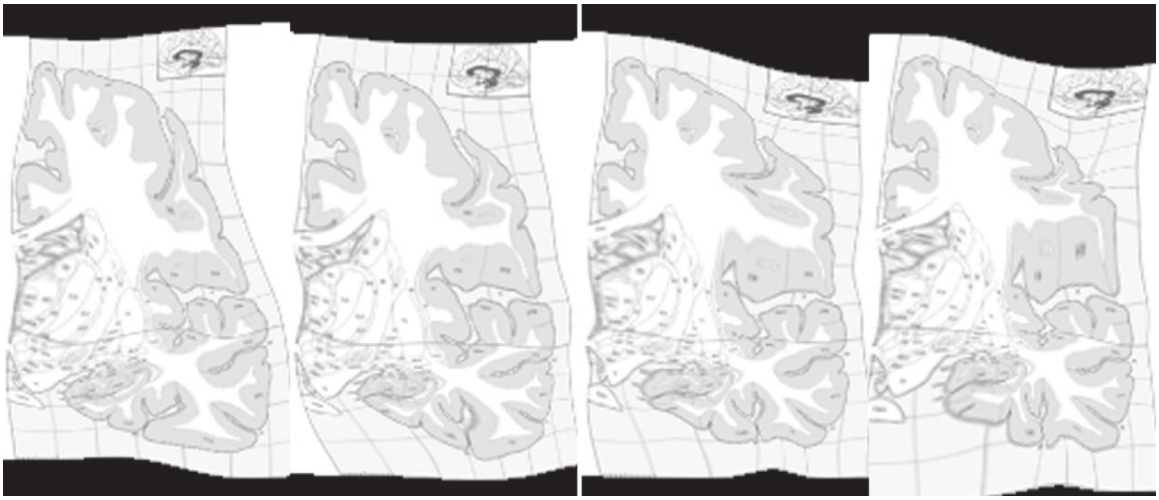

Figure 9: Warped Atlas images. Four warped atlas images with different numbers of control points (25, 35, 25, 50 from left to right)

Appendix 2: Neuronal Efferent and Afferent Trajectories

As described in the text, non-human primate histological studies have shown that Vim thalamocortical neurons project to primary motor cortex (Hoover and Strick 1999), while Vc thalamocortical relay neurons terminate in the somatosensory cortex (Darian-Smith et al. 1999; Kultas-Ilinsky et al. 2003). We modeled these thalamocortical efferent projections based upon reconstructions of biotinylated dextrane amine labeled neurons to the macaque motor cortex and cat motor cortex and subsequent 3-D reconstruction methods (Darian-Smith et al. 1999; Kakei et al. 2001) . The figures below, as found in the published papers illustrate the model.

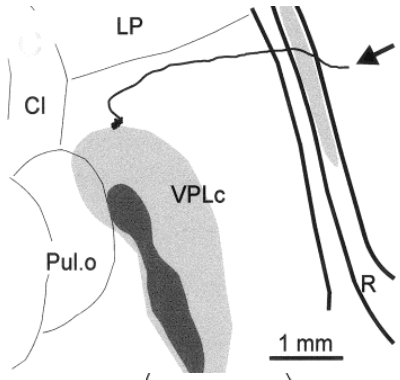

Figure as published by Darian-Smith et al in *The Journal of Comparative Neurology* , 410: 225 (Darian-Smith et al. 1999). Pul.o-anterior pulvinar nucleus; Cl, central lateral nucleus; LP-lateral posterior nucleus; R-thalamic reticular nucleus

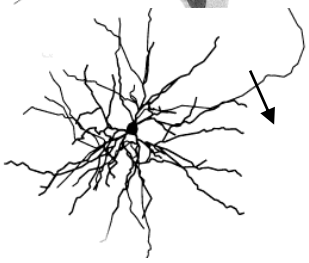

Figure as published by Darian-Smith et al in *The Journal of comparative neurology*, 410: 215 (Darian-Smith et al. 1999). Arrow points at axon traced a short distance out of the Pulvinar nucleus of thalamus.

The efferent path to cortex coursed along a medial-ventral to lateral-dorsal angle in the coronal plane and posterior-ventral to anterior-dorsal angle in the sagittal plane (Kakei et al. 2001).

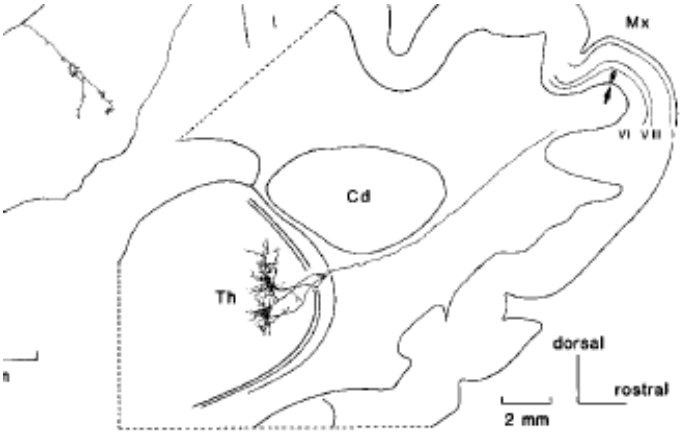

Figure as published in Kakei et al in *The Journal of comparative neurology*, 437: 179 (Kakei et al. 2001). Th, thalamus; Cd, caudate nucleus

While the tracing studies were performed to analyze corticothalamic projections from motor cortex to thalamus, studies have also demonstrated a reciprocal relationship between corticothalamic neurons and thalamocortical neurons (Sherman and Guillery 1996). Based on this relationship, the thalamocortical projections in this study were modeled with a 25 degree angle from the intercommissural plan in a coronal

slice and a 45 degree angle from the intercommissural plane in a sagittal slice. Additionally, the Matlab algorithm allowed for a 10 degree randomized angle orientation in both planes. For the purpose of this study, the same neuron orientation was used for both Vim and Vc efferent neurons given the consistent anterior-posterior relationship between their motor cortical targets (Mai et al. 2008).

The afferent trajectory used in this study, as described in the text, was based on a previous histological staining study in humans. An image from this study is illustrated below including the cerebellothalamic tract. Based on the results from this study, the model proposed in our study followed that the cerebellothalamic tract was found to enter thalamus at an angle of approximately 45° with the intercommissural plane in the coronal slice. Moreover, in the sagittal plane, the entrance to Vim and Vc thalamus followed a 60° angle with the intercommissural plane (Gallay et al. 2008).

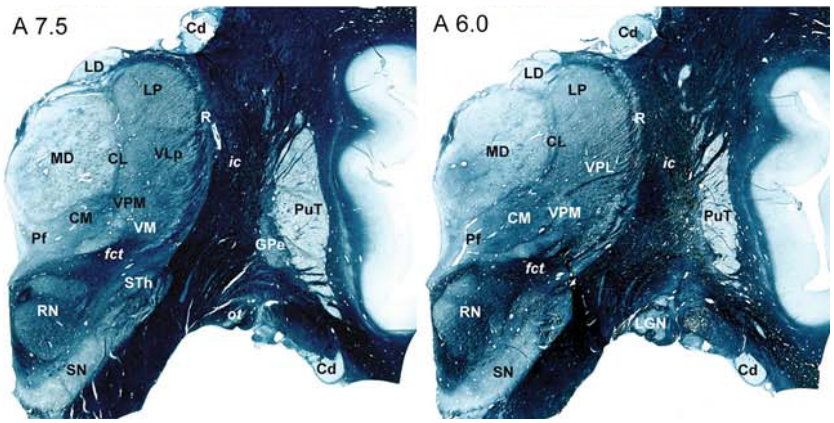

Figure as published by Gallay et al in *Brain structure & function*, 212: 447 (Gallay et al. 2008). Cd, caudate nucleus, LD, lateral dorsal nucleus; LP, lateral posterior nucleus; R, reticular thalamic nucleus; CL, central lateral nucleus; VPL, ventral posterior lateral nucleus; VPM, vetral posterior medial nucleus; CM, centromedian nucleus; Pf, Parafascicular nucleus; fct, cerebellothalamic tract; RN, red nucleus; SN, substantia nigra; Put, putamen; LGN, lateral geniculate nucleus;

Appendix 3: Neuronal Activation for each Lead Corresponding to DBS Outcome

Table 2: Lead 1 Neuronal Activation Profile

Lead 1 Neuronal Activation						
Stimulation Setting		**Activation of Neuronal Population**				**Stimulation Outcome**
Contact	Cathode Voltage (V)	Vc Efferent	Vc Afferent	Vim Efferent	Vim Afferent	Clinical Notes
C3	1	1.98	4.37	16.071	47.42	some improvement, no side-effects
	2	13.89	21.07	23.016	76.59	complete improvement
	4.5	21.83	36.38	33.532	95.24	persistent paresthesias in jaw and right upper extremity
C2	1.5	14.09	17.2	12.698	54.65	complete improvement
	2	15.28	18.06	15.278	81.94	complete improvement (final setting)
	3	18.25	21.43	19.444	88.89	persistent paresthesias
C1	1.5	11.90	12.50	6.944	68.65	complete improvement
	2	14.09	18.06	9.524	84.33	transient tingling and numbness in jaw and right upper extremity
	2.5	15.28	21.03	10.714	90.48	persistent paresthesias in jaw and right upper extremity

Table 3: Lead 2 Neuronal Activation Profile

Lead 2 Neuronal Activation						
Stimulation Setting		**Activation of Neuronal Population**				**Stimulation Outcome**
Contact	Cathode Voltage (V)	Vc Efferent	Vc Afferent	Vim Efferent	Vim Afferent	Clinical Notes
C0	1	5.95	4.37	1.984	44.44	some improvement, no side-effects
	1.5	7.54	13.49	3.175	86.31	persistent tingling and numbness in arm and jaw
C3	1.5	0.00	1.99	9.200	31.20	complete improvement in postural tremor
	2	0.40	26.44	21.000	45.40	tingling and numbness with facial droopiness and slurred speech
	2.5	3.98	41.35	30.600	61.40	threshold for persistent paresthesia
C2	1	0.00	0.99	7.000	24.40	complete improvement in tremor (better than C0 and C1)
	2	7.75	35.19	23.60	55.00	tingling and numbness
	2.5	15.31	59.76	28.200	68.20	persistent paresthesia
C1	1	1.99	13.12	11.200	28.40	significant improvement in postural tremor (with intentional component)
	2	16.10	31.41	17.60	64.00	2.0 tingling and numbness
	2.5	19.28	33.80	17.600	76.80	persistent paresthesia
C0	1	6.56	17.26	8.400	29.40	some improvement in tremor, no side-effects
	1.5	9.54	22.82	10.400	47.40	tingling and numbness
	2	12.33	27.38	12.600	68.40	persistent paresthesia

Table 4: Lead 3 Neuronal Activation Profile

Lead 3 Neuronal Activation						
Stimulation Setting		**Activation of Neuronal Population**				**Stimulation Outcome**
Contact	Cathode Voltage (V)	Vc Efferent	Vc Afferent	Vim Efferent	Vim Afferent	Clinical Notes
C3	2	0.40	20.83	6.548	75.20	improvement in postural tremor
	6.5	1.58	66.87	49.206	100.00	tingling and numbness in his right arm
C2	2	0.20	20.04	5.357	68.85	improvement in tremor
	4.5	2.38	68.77	13.095	96.43	persistent tingling and numbness in his right arm and throat
C1	1.5	0.20	8.73	2.579	50.40	some improvement in postural tremor, with no side effects
	2	0.40	15.08	3.571	85.52	good improvement in postural tremor, with no side effects
	3	0.40	23.02	5.159	96.03	persistent tingling and numbness in his right hand
C0	1.5	0.20	6.55	0.397	56.94	improvement in tremor, no side-effects
	2	0.40	10.12	1.389	85.91	persistent tingling and numbness in his right arm

Table 5: Lead 4 Neuronal Activation Profile

Lead 4 Neuronal Activation						
Stimulation Setting		**Activation of Neuronal Population**				**Stimulation Outcome**
Contact	Cathode Voltage (V)	Vc Efferent	Vc Afferent	Vim Efferent	Vim Afferent	Clinical Notes
C3	0.5	0.00	4.76	8.730	52.98	no improvement in tremor, no side-effects
	1	0.20	15.28	11.706	75.40	no improvement in tremor, transient tingling in teeth
	1.5	1.59	29.17	13.294	87.30	improvement in postural tremor, mouth tingling
	2	7.34	44.25	14.683	95.83	minimal improvement in tremor, speech difficulties
	2.2	8.13	46.23	14.881	96.23	minimal improvement in tremor, slow speech, hesitation
C2	0.5	0.20	6.01	3.968	51.98	slight improvement in tremor, no side-effects
	1	0.20	12.50	6.548	75.79	slight improvement in tremor, no side-effects
	1.5	1.98	34.23	7.937	86.90	slight improvement in tremor, transient tingling, slow speech
	2	4.37	38.10	8.929	95.63	unable to speak, anxious
C1	1	0.20	9.92	1.587	82.54	no improvement in tremor, mild tingling
	1.5	0.20	17.66	2.579	91.27	slight improvement in tremor, tongue tingling, slurred speech
	2	1.79	38.69	3.373	99.60	unable to speak, anxious
C0	1	0.00	18.06	0.000	86.90	mild improvement in tremor, difficulty speaking
	1.5	0.00	25.40	0.000	96.03	pulling lip, tingling in arm, leg, couldn't speak
C2 - C3 +	0.5	0.20	1.59	4.960	34.13	no improvement in tremor, no side-effects
	1	0.40	5.36	9.722	55.75	no improvement in tremor, no side-effects
	1.5	0.79	7.94	14.484	68.65	no improvement in tremor, no side-effects
	2	1.19	13.89	18.056	80.36	no improvement in tremor, no side-effects
	2.5	2.78	22.02	20.437	86.51	some improvement in tremor, no side-effects